Revealing Dusty Star-Forming Galaxies in a Galaxy Cluster in Formation in the Early Universe

Armando Delgado Fumero

Science Faculty, Physics Section

Supervisor: Helmut Dannerbauer

September 2018

Contents

1 Abstract **5**

2 Introduction **6**

2.1 Resumen 6

2.2 Basic knowledge 6

2.2.1 Galaxy Clusters 7

2.2.2 Dusty Star Forming Galaxies 7

2.3 Instrumentation 8

2.3.1 APEX 8

2.3.2 LABOCA 9

3 Objectives **11**

3.1 Resumen 11

3.2 Objectives of the project 11

4 Methodology **12**

4.1 Resumen 12

4.2 Software used 12

4.2.1 Crush 12

4.2.2 DS9 13

4.3 Data reduction 13

4.3.1 First method 15

4.3.2 Second method 18

5 Results **20**

5.1 Resumen 20

5.2 Image smoothing 20

5.3 Source extraction 21

6 Conclusions **25**

6.1 Resumen 25

6.2 Conclusions 25

A Data tables **26**

B Scripts **30**

B.1 Crush script 30

B.2 Detect script 31

B.3 Selection script 33

List of Figures **35**

Bibliography **36**

Chapter 1

Abstract

Este trabajo consiste principalmente en el procesamiento y análisis de imágenes obtenidas mediante el telescopio APEX (Atacama Pathfinder EXperiment), particularmente las obtenidas por el dispositivo LABOCA (The Large Apex BOlometer CAmera). La zona observada que usaremos para realizar el estudio es la correspondiente al recientemente descubierto cúmulo SpARCS J0224727032354 con redshift z = 1.63, lo cuál corresponde a aproximadamente el 29% de la edad del Universo. El objetivo último de esta investigación es estudiar la formación de galaxias y como tienden a estructurarse estas en sus etapas más prematuras. Sabemos que las galaxias tienden a agruparse en cúmulos y protocúmulos por simple gravedad pero históricamente se creía que esto ocurría en etapas más tardías de su evolución. Recientemente se ha descubierto que muchos de estos cúmulos se crean en etapas muy tempranas de la vida de las galaxias. Para observar esto estudiamos galaxias en el lejano Universo, donde las observamos en las etapas más iniciales de su evolución. Debido a la extrema lejanía de estos objetos celestes, no somos capaces de observar mucho de ellos, sin embargo, sabemos que estas galaxias tienden a tener mucho polvo en sus inmediaciones. Ese polvo se ve recalentado por la cercanía a estrellas productoras de calor, creando superficies muy grandes con una temperatura muy superior a la del vacío. Para observar esto estudiamos su emisión en un intervalo conocido como FIR/submm, situado en longitudes de onda de entre 200μm y 1mm.

La reducción de datos se realiza mediante el programa 'Crush', desarrollado por A. Kovacs y nos apoyamos también en el programa 'DS9'.

Una vez hemos reducido los datos estudiamos la cantidad de miembros visibles del cluster en esta longitud de onda y la posibilidad de que estos datos sean verídicos con las herramientas que tenemos a nuestra disposición. Primeramente intentamos una reducción demasiado refinada para la calidad de nuestros datos, que resulta errónea. Finalmente, con un procesamiento de menor resolución obtenemos un resultado aceptable, obteniendo al menos 1 fuente robusta y 4 tentativas.

Chapter 2

Introduction

2.1 Resumen

En esta sección se muestran los argumentos teóricos básicos usados para realizar el estudio y la instrumentación usada para obtener los datos.

Dada nuestra corta esperanza de vida comparada a la vida de cualquier objeto celeste, ya sea una estrella o un conjunto de objetos como pueden ser galaxias, protocúmulos o cúmulos, no tenemos formas de ver como evolucionan. Por tanto, para estudiar estos objetos en sus etapas más primigenias necesitamos observarlas en el lejano unverso, debido a que sabemos que espacio y tiempo son proporcionales (a mayor distancia se encuentre un objeto lejano estaremos viendo una versión más vieja de éste). En nuestro caso estudiamos "submm galaxies", llamadas así porque se estudia su emisión de calor en longitudes de onda de entre 1mm y 200μm. Para ello utilizamos datos obtenidos por el telescopio APEX (Atacama Pathfinder EXperiment), particularmente las obtenidas por el dispositivo LABOCA (The Large Apex BOlometer CAmera). Este sensor detecta ondas del ancho de banda anteriormente mencionado. APEX fue construido por un conglomerado de organizaciones liderado por el MPIfR (55% en propiedad), OSO (13%) y ESO (32%), donde España participa. LABOCA es un dispositivo llamado "array bolometer" compuesto por 295 canales, situados de forma concéntrica alrededor de un canal central. Trabaja en la ventana atmosférica de 870μm y la luz llega al dispositivo tras pasar por un complejo sistema óptico parte del telescopio.

2.2 Basic knowledge

We do not live long enough to see how celestial objects evolve and structure themselves. To solve that, we study different objects in different states of its evolution. In this case we study the far Universe to check the early states of clusters and how galaxies group themselves. Redshift is the usual measure used to size the age of these objects, and it comes from the physical phenomenon known as Doppler effect (shown on equation 2.1, where ν is frequency of a moving object, ν_o original frequency, v is the velocity and c is speed light). Since the Universe is expanding, the radiation that arrives at us will have different values of frequency/wavelength depending how far they are from us (distance is related to its relative velocity respect to us).

$$\nu = (1 + \frac{\Delta v}{c})\nu_o \tag{2.1}$$

For example, seeing objects at red shift z<1 mean we are seeing things that happened when the Universe had less than half of its actual age (Lineweaver et al., 2003). To estimate this data we start from Friedmann's equation and operate until we get equation 2.2. We neglect energy density and we consider Universe to be flat. We use Hubble Constant $H_o = 68.14 \frac{km}{s*Mpc}$, Omega matter $\Omega_M = 0.3036$ and, since we consider Universe to be flat, $\Omega_\Lambda = 0.714$.

$$t = \int_0^{\frac{1}{1+z}} \frac{da}{H_o(\frac{\Omega_M}{a} + a^2\Omega_\Lambda)^2} \tag{2.2}$$

We are going to study the cluster SpARCS J0224727−032354 with redshift z = 1.63. Therefore we will be looking at a zone of the universe with an age of approximately 4100 Gyr (using equation 2.2), 29.5% of the actual age of the Universe. Our work start from the proposal for observations made by Demarco and Dannerbauer. SpARCS J0224727−032354 is a recently discovered where there have been identified 23 members using NIR/optical methods. There are evidences of merging activity on large-scale structures and the photometric data show a young red sequence and a large proportion of optically red star-forming galaxy. LABOCA is an ideal instrument to study massive galaxies in formation, that will be the main object of study, so the proposal asked for 25 hours of observation.

2.2.1 Galaxy Clusters

Historically, it is been thought that most galaxies at high-z are usually galaxies in relative isolation, but observations in the last 20 years have identified an important amount of galaxies tending to merge into conglomerates of galaxies called proto-clusters. We may define proto-cluster as a macro-structure composed of galaxies bound together by gravity. In later phases of the stellar evolution it is known that galaxies are usually members of these macro-structures (we may define them as proto-cluster or cluster depending on the grade of stability they acquire, where proto-clusters are non-viralized and clusters are viralized) but only recently it is been studied this early grouping (Dannerbauer et al., 2014).

2.2.2 Dusty Star Forming Galaxies

Since these macro-structures are still in a building phase there is a lot of interstellar dust around (Casey et al., 2014). More specifically, it is thought that gas-rich disk galaxies collide and proceed to ignite phases of star formation by the rapid compressing and cooling of gas. This collision and subsequent star formation triggers the prolific formation of dust particles (Casey et al., 2014). This dust gets heated due to their proximity to diverse stars and their own nature. The contrast between these dusty galaxies and the vaccum that surrounds them allows us to detect them. 99% of the energy released by those galaxies are produced by thermal emission (Blain et al., 2002) from their dust grains. First DSFG (Dusty Star Forming Galaxy) identified as part of a proto-cluster was LAB1 at z=3.09 (Chapman et al., 2001) and since that day until now nearly a million DSFGs have been detected (Casey et al., 2014).

Since we are studying the heat these objects emit we must take into account the basic law that relates energy and heat. That is Planck's law, that let us we know that the energy irradiated by an ideal black body is directly related to the temperature this body has. We have I_λ ($\frac{W}{sr*m^2*Hz}$), as the spectral radiance emitted by a black body, h as Planck's constant ($6.62610^{34} J*s$), λ as the wavelenght, Boltmannz's constant as K_B ($1.3810^{-23} J/K$) and c as light speed ($3*10^8 m/s$).

$$I_\lambda = \frac{2\pi hc^2}{\lambda^3 * (e^{hc/K_B\lambda * T} - 1)} \tag{2.3}$$

Having this law into account (on its Rayleigh-Jeans approximation $I_\lambda(T) = \frac{2*c*K_B*T}{\lambda^4}$) we may study these galaxies. These galaxies are called "SMG", acronym for submillimeter galaxies. This name refers to the fact that they are discovered in submillimiter wavelengths, between 200μm and 1mm (Blain et al., 2002). All of the DSFG in the Universe produce an infrared radiation field that has an equal energy density as the direct starlight eission from all galaxies visible at ultraviolet and optical wavelengths (Casey et al., 2014). Grains are heated to temperatures between 20K and 200K depending on the interstellar radiation field and the size and optical properties of the grains (Blain et al., 2002). The main parameter to study this heat is the emission spectrum and its simplest form is given by asumming $f_\lambda \, \alpha \, [1 - exp(-\tau_\lambda)]I_\lambda$, where the emitting source is understood as optically thin. I_λ is Planck's function, τ_λ is the wavelength-dependent optical depth of the cloud (multiple of ϵ_λ) and f_λ is the emission spectrum (Blain et al., 2002).

2.3 Instrumentation

2.3.1 APEX

APEX (Atacama Pathfinder EXperiment) was built in 2004 due to collaboration between the Max Planck Institut für Radioastronomie (MPIfR) at 55%, which is the main organization owner of this project, the Onsala Space Observatory (OSO) at 13%, also known as Swedish National Facility for Radio Astronomy and ESO (European Southern Observatory) at 32%, a consorcium of several european countries (including Spain) that works Astronomy in the southern observatory. The telescope is located in the Atacama desert, Chile, at an altitude of 5000m, in the same place other telescopes with similar properties are placed too, such as ALMA ("Atacama Large Millimeter/submillimeter Array", APEX is in fact an ALMA prototype), thanks to the ideal weather for the astronomycal observation (extremely dry).

Figure 2.1: Apex Telescope

This 12m diameter telescope is composed of several devices, including heterodyne systems and bolometer arrays. For this study we use data obtained from LABOCA, the main bolometer array of this telescope.

2.3.2 LABOCA

LABOCA (Siringo et al., 2009) is the instrument used to obtain the data we will use for this study. it is a multi-channel bolometer array for continuum observations that operates at 870 μm (345 GHz). It consists of 295 channels, which are arranged in 9 concentric hexagons around a central channel. It has an angular resolution of $18.6''$ and a total field view of $11.4'$. Once the channel separation is the double of the beam size (around $36''$) the array is under-sampled and special techniques are used to obtain full sampled maps in a time-efficient manner.

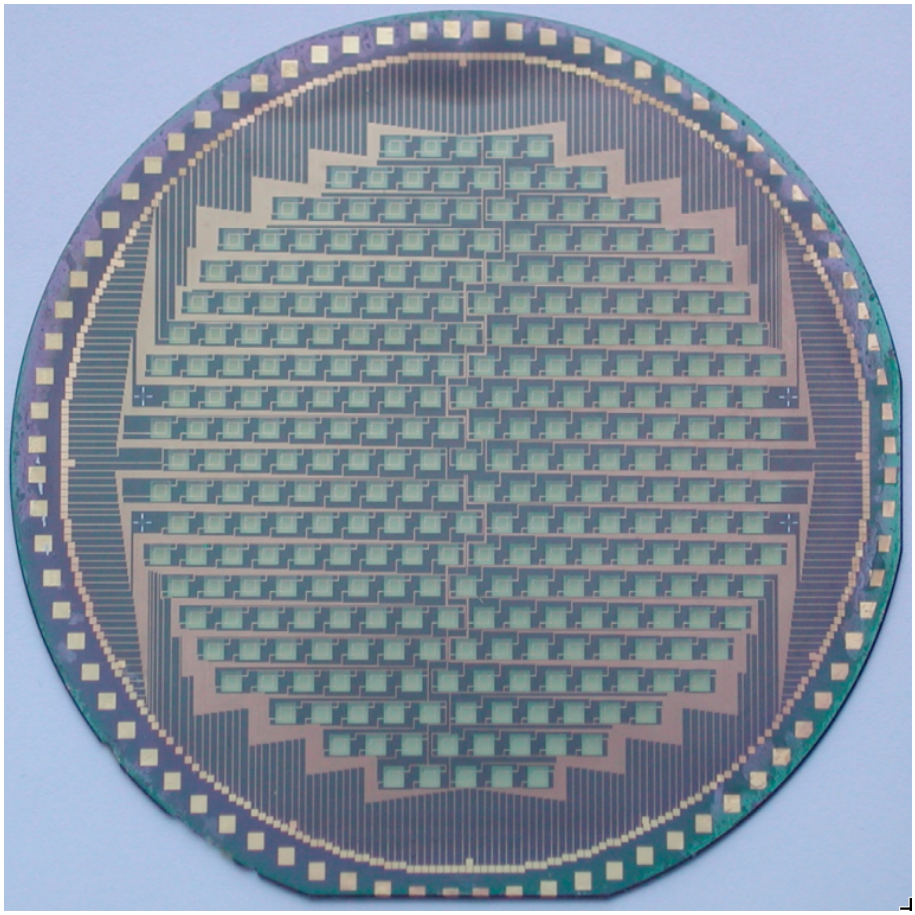

Figure 2.2: LABOCA bolometer array.

The radiation that arrives at APEX is absorbed by a thin metal film extremely cooled (around 280mK). The more radiation it receives the more the temperature rises. These variations are measured and translated into a voltage change that is amplified and measured again.

After the radiation is reflected by the primary (main dish) and secondary (sub-reflector) mirror, a rather complicated tertiary optics is needed to illuminate LABOCA's focal plane.

Finally, the radiation enters through an active window into the cryostat and, after passing through the passband filters, is collected by an array of conical horn antennas, before it reaches the bolometers

The bolometers are both AC-biased (AC signal produced by the signal received superposed over a current DC voltage using an inductive system) and DC-coupled (Direct Coupling, AC signal is transmitted via physical contact), making LABOCA a total power detector. The system is designed to work at a frequency of 345 GHz (approximately 870μm) with a bandwidth of about 60 GHz, which matches the atmospheric window (portion of the electromagnetic spectrum that can be transmitted through the atmosphere without any distortion or absorption). Bolometers are pure broadband-continuum detectors, they do not provide any spectral information, but do surpass heterodyne systems (the other kind of device installed in this telescope) by far in terms of continuum sensitivity.

To secure these extremely low temperatures (under 300mK) there is a protocol to be followed. First, LABOCA is enclosed in a commercial 20-cm cryostat accomodated at the MPIfR to accomodate a double-stage sorption cooler and the rest of the components of the device.

The cryostat incorporate a 3-liter reservoir of liquid nitrogen and a 5-liter reservoir of liquid helium. After producing a high vacuum of around 0.0001 Pascals (9.8692e-10 atm) the cryostat is filled with the liquid cryogens. Nitrogen provides temperature shielding of around 74K (in this location due to its altitude) and the helium shields a temperature of 3,7K. This system must be refilled once per day.

The second part of the temperature protocol is the sorption cooler. A LABOCA is enclosed in a high-vacuum cryostat using liquid nitrogen and liquid helium in a combination with a two-stage sorption cooler. A 3-L reservoir of liquid nitrogen provides through evaporation a thermal shielding at 73.5 K temperature at the high-altitude site of APEX. Inside that, a 5-L tank of liquid helium provides another thermal shielding at 3.6 K temperature. The final push to get the 250 mK is done by the sorption cooler using both helium-4 and helium-3. The operational time of LABOca is limited by these restrictions, being the maximum uninterrumpted time of observation around 11 hours, after which a recycling is necessary.

Chapter 3

Objectives

3.1 Resumen

Este trabajo de fin de grado tiene como objetivo estudiar la evolución de las galaxias y las agrupaciones de estas, particularmente estudiando las imágenes obtenidas por LABOCA del recientemente descubierto cúmulo SpARCS J0224727−032354 con redshift z = 1.63. Este cúmulo tiene 23 miembros descubiertos y se cree que está en mitad de un proceso de unión de varios de estos miembros. Los datos con los que trabajamos tiene una calidad que debería ser suficiente para permitirnos encontrar alrededor de 5 SMGs. Nuestro trabajo consistirá en buscar galaxias "submm", utilizando las diferentes configuraciones que permite el software 'crush' para obtener imágenes con un ruido que asegure la fiabilidad del resultado. Una vez se haya obtenido el mejor resultado posible deberemos extraer las fuentes que se observan en él y crear un catálogo.
Como objetivo secundario se tiene el automatizar el proceso de procesamiento y análisis de datos para futuras ocasiones.

3.2 Objectives of the project

This project is aimed to study the evolution of galaxies and how they group, particularly studying images obtained by LABOCA from he recently discovered cluster SpARCS J0224727032354 with redshift z = 1.63. This cluster is supposed to have 23 members and is believed to be in a process of merging activity along a young red sequence. The data we have has a deepness that should suffice to see around 5 of these members.
Our job will consist on searching submm galaxies, processing the images obtained by the LABOCA camera using the different options the program 'crush' provides us until we find the optimal one. Once we've got the best possible image based on the noise present on it we have to extract the sources, providing a reliable catalog.
There is a secondary task which consists in automatizing the processing and analysis of the data for future times.

Chapter 4

Methodology

4.1 Resumen

En esta sección se tratara el método utilizado para obtener el resultado final, incluyendo las herramientas informáticas usadas y el método de trabajo.

Empezamos tratando el software usado. Para analizar las imágenes del 'bolometer array' de APEX usamos un programa desarrollado por Attila Kovacs (Computer Enginner at the Smithsonian Institute for Astrophysics) llamado 'Crush'. Este programa está específicamente diseñado para procesar datos obtenidos de 'submilimiter wave cameras'. Como viene en su descripción, está preparado para ser utilizado en varios de los principales artefactos de este estilo como SHARC, LABOCA, ASZCA, GISMO... La otra herramienta informática que usaremos es DS9, desarrollada por el Smithsonian Institute for Astrophysics, nos permite leer los archivos fits y cambiar características de la visualización de la imagen como brillo y contraste.

Una vez se ha presentado el software especificamos su uso. Primero probamos las diferentes configuraciones posibles de crush. Por las características de las imágenes descubrimos que el sistema adecuado es 'deep', correspondiente a imágenes muy débiles. Una vez tenemos claro esto, procesamos todas las imágenes por separado. Ahora que tenemos todas las imagenes individualmente procesadas usamos la herramienta 'detect', de 'crush' para ver el ruido correspondiente a cada una de ellas. También usamos DS9 para asegurarnos que estas imágenes no tienen anomalías y que el ruido de la imagen es el esperado. Con los datos obtenidos en este proceso procedemos a realizar las imágenes finales.

A partir de los datos obtenidos por el análisis previo filtramos los archivos a usar para la imagen final según su ruido y la presencia de anomalías y obtenemos varias posibles imágenes finales. Analizando principalmente el ruido y la ubicación de las fuentes (proporcional al ruido) entre estas imágenes finales elegiremos la mejor.

4.2 Software used

4.2.1 Crush

Crush (`http://www.sigmyne.com/crush/`) is the name of the program used to process the data. It was developed by Attila Kovacs (Computer Enginner at the Smithsonian Institute for Astrophysics) as a PhD project (Kovacs et al., 2006) (Kovacs et al., 2008) and he has carried on updating it since then as the

program has remained extremely useful due to its speed, versatility and efficiency. Written in Java, it is available for almost every operative system. It has several functions. First and most important, it is able to process and reduce astronomical imaging arrays. One of the main important points of this program is that allows the user to process more than image at a time, reducing as many images as you want into one file. It can process data from several bolometer systems such as SHARC, SHARC-2, LABOCA. SABOCA, ASZCA, p-ARTEMI, PolKa, GISMO, MAKO, MAKO-2, SOFIA/HAWC+, MUSTANG-2, SCUBA-2 and SOFIA/HIRMES. Besides reducing data from bolometer arrays, it has other features such as "imagetool" (feature that allows you to manipulate images), "show" (simple display program for fits files), "coadd" (mixing FITS images together), "difference" (checks differences between two images), "histogram" (writes histogram of the pixel distribution of an image plane), "detect" (source extraction tool for maps) and "esorename" (renames ESO files to their original names). This software is meant to be run under terminal and it has no graphic interface (except "show").

4.2.2 DS9

DS9 (`http://ds9.si.edu/site/Home.html`) is an astronomical imaging and data visualization application that supports FITS images, multiple frame buffers, region manipulation, and many scale algorithms and colormaps. It is a program that allows us to sort out the images we may know wrong with a simple look at them thanks to the manipulation of visual characteristics. It also will provide us a tool to create .reg files that will be used later to point the possible sources. This program is developed by the Smithsonian Astrophysical Institute.

4.3 Data reduction

When we start this study we are given 270 FITS files. Those files are the result of 3 nights (27, 28 and 29 July 2015) of continuous observation on the zone of the sky that interests us. From those 270 files, 134 are science and calibration files. Therefore, the number of files to use on our study will be 136.

Once we have set this data we have to process them. For that instance we use the program 'Crush'.

First, we process individually some of those files under different configurations. These configurations depend mainly on the S/N of the FITS files, we start doing the general processing, with no extra options. Then we use other options such as 'bright' that is aimed for large S/N, 'faint' (low S/N) and 'deep' (really low S/N and point-like sources). We might combine those options with the 'extended' setting if we suspect there is an extended structure. We can also combine those options between them. We can see some examples in the Fig 4.1.

Every one of the files have really low S/N so the correct setting to use is 'deep'. This is something known before trying the different configurations (we can see FITS properties on software like IRAF, Astropy or DS9), but we check them anyway to make sure. On some cases we might use the 'extended' option but it not really necessary overall.

Now we process all the files of our set with the selected configuration. For that purpose we may automatize it using a python script (Appendix B1). Once every individual image is processed we check them using another 'Crush' feature, 'Detect'. With this feature we measure the noise. For that purpose we may use another python script (Appendix B2) that will print the 'Detect' results of every processed file on one take, since 'crush' only allows doing it one file at a time.

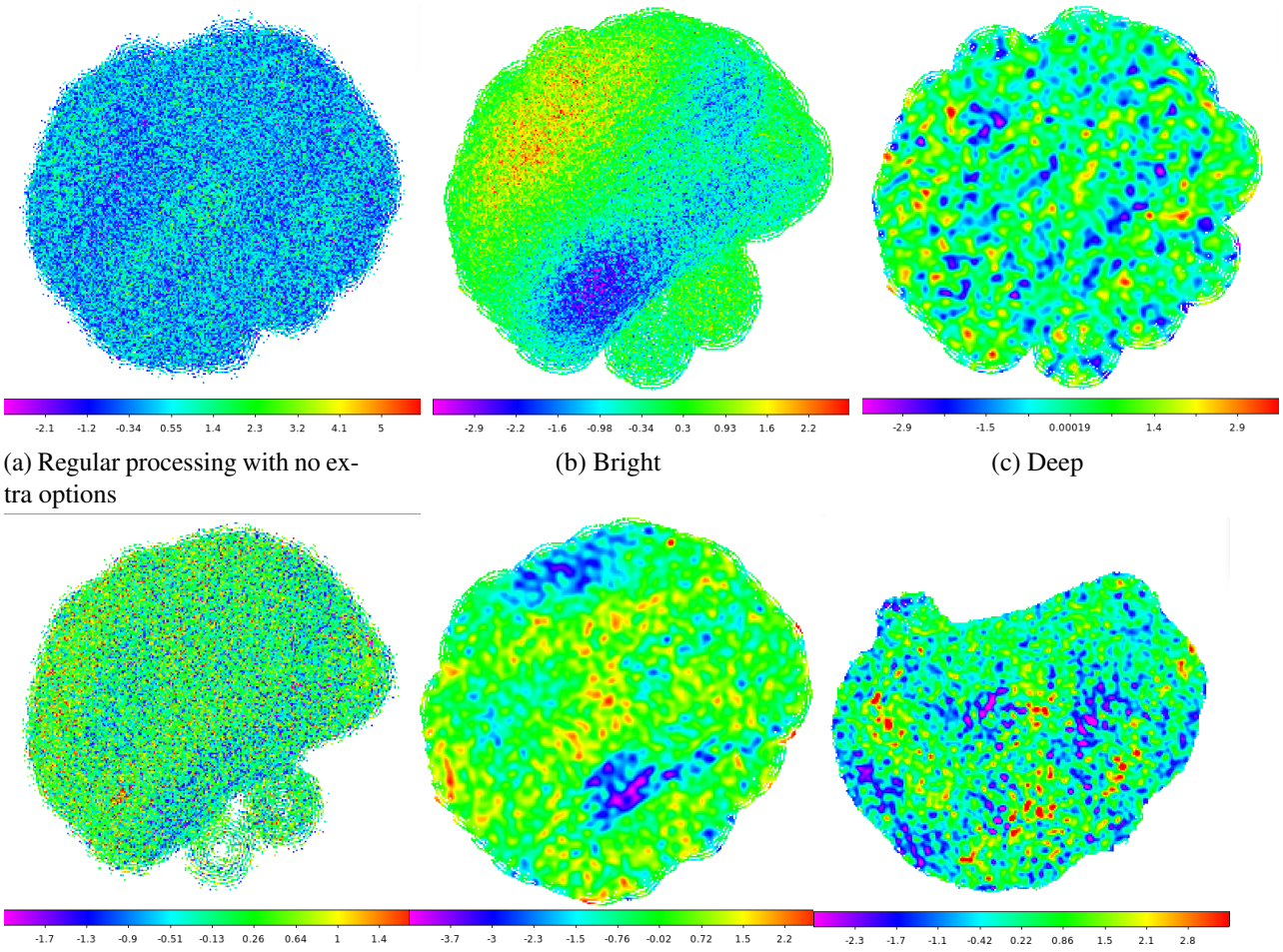

(a) Regular processing with no extra options

(b) Bright

(c) Deep

(d) Extended

(e) Extended, Faint, Deep

(f) Faint

Figure 4.1: APEX-45439 file, processed through different options

We check these images not only with 'Detect' but also with the other software mentioned before, 'DS9'. We do this to check the noise in the image as a whole. We can see on Fig 4.2 an anomaly in the image that could alterate the final images, but since it does not have any source peak on it, 'detect' would not get a hold of it (since we use a 'detect' configuration to see the peaks). We check every image individually and make sure those images have no strange features and the noise through the whole image is not too high. We save this data in 3 columns. First column will be 'Detect' noise, where we save the maximum noise value we get from a peak on the 'detect' print, usually this data will be the corespondent to peaks located in the sides of the image, where noise is really big. Using this Data, we will know how noisy can a image get. 'DS9' noise is the second column, where we save the minimum noise value we get on every picture checking manually with 'DS9'. We use both "'detect' noise" and 'DS9 noise', so we have a good measure of noise both in the center and the sides of the image. As third column we have 'Comment', where we will simply write down if there is an anomaly, a zone of extreme noise that does not follow the patterns of noise expected in these files ("Wrong" if there is a noisy feature, "Correct" if there is not).

We will use this info later to create the final image in addition to a fourth column, the tau mean of every set of files (data we get from `http://www.apex-telescope.org/bolometer/laboca/calibration/opacity/`). Tau is the measure used in astrophysics for optical depth, the air quality

at that moment in the sky. It is not very relevant in this study since all tau values on these files are good.

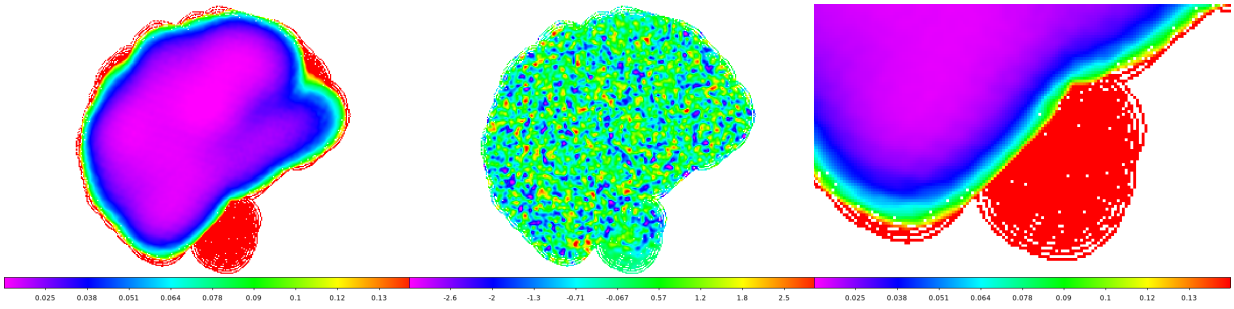

(a) Noise (b) Signal to noise (c) Noisy anomaly

Figure 4.2: Anomaly on APEX-45436

4.3.1 First method

The final image will come from using different ranges of noise using the data table (visible on Appendix A). We use another python script (Appendix B3) that picks the files that match the restrictions we want, based on the different measures done before. We set different values for these enquiries in order to get the best result possible based on the noise these images have.

First, we can see on Fig 4.3 a processing based on all files (128 of the original 136 files, the other 8 were corrupt).

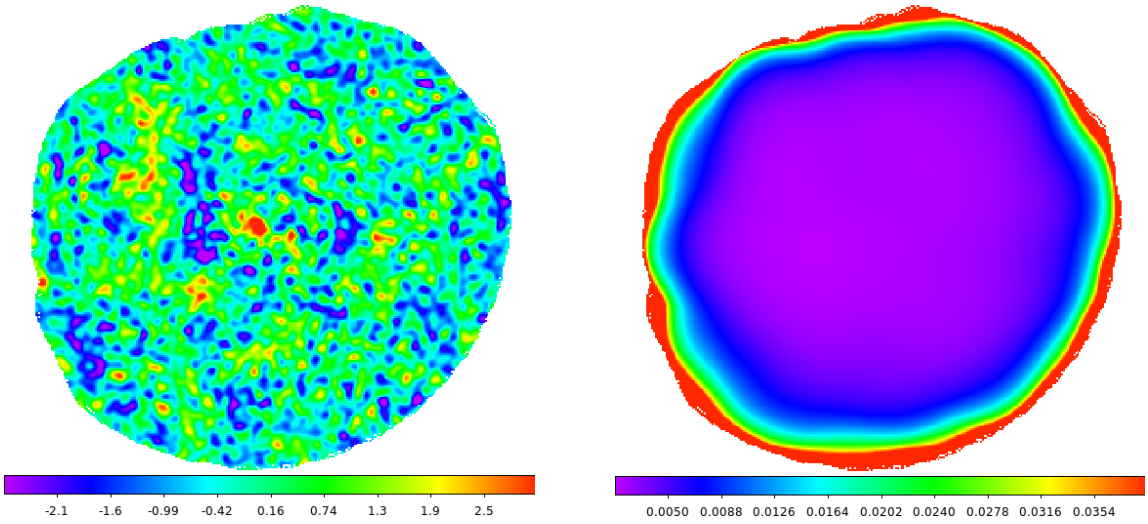

(a) Signal to Noise (b) Noise

Figure 4.3: Processing using all files

Next, Fig 4.4 is processed based on the files that have no anomalies and it is not based on the noise values for a total of 73 files. We see less peaks, and the ones we see are central and its values rise above the rest of the image.

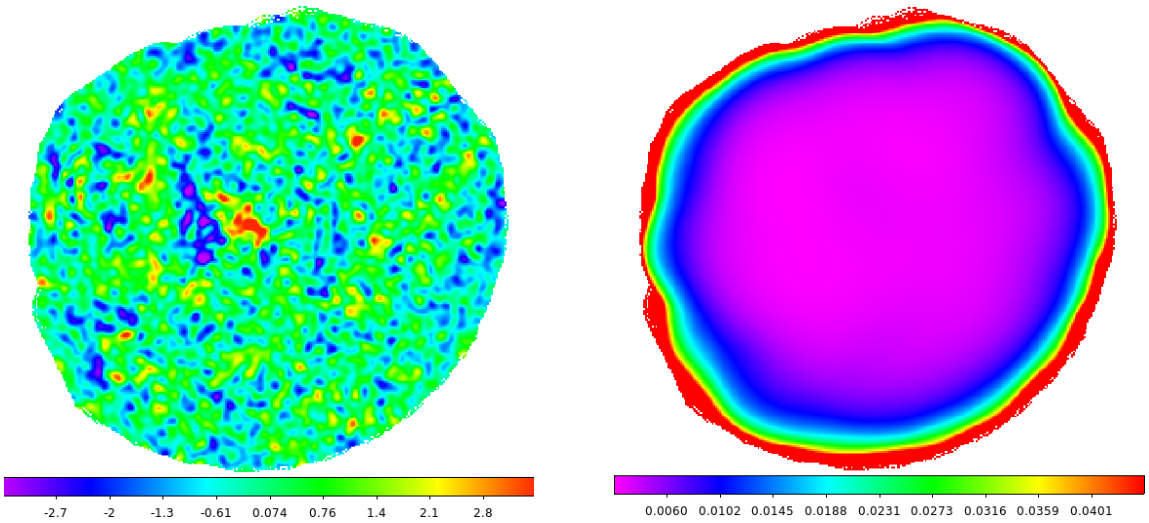

(a) Signal to Noise (b) Noise

Figure 4.4: Processing using all files that present no anomalies

This one, Fig 4.5, has restricted vales for 'DS9' noise and 'Detect' noise, having 0.018 Jy/beam and 0.09 Jy/beam as maximum values respectively. We use 69 files this time, just 4 less due to the non-restrictive noise range used so it is pretty similar than the previous one, showed on Fig 4.5.

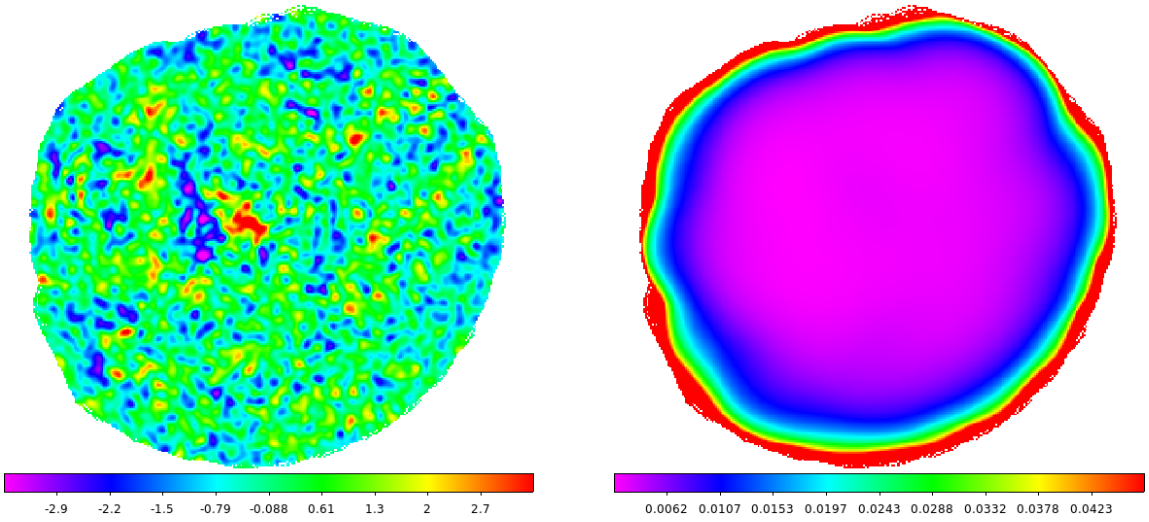

(a) Signal to Noise (b) Noise

Figure 4.5: Processing using files that present no anomalies, 'DS9 Noise'<0.018, 'Detect Noise'<0.09

Now we have Fig 4.6, that shows an image obtained from a 0.017 Jy/beam and 0.07 Jy/beam restriction. We use this time 51 files and we can see noise stays almost identical through these 4 pictures.

Finally we have a 0.015 Jy/beam and 0.05 Jy/beam limits for Fig 4.8. Due to the really low num-

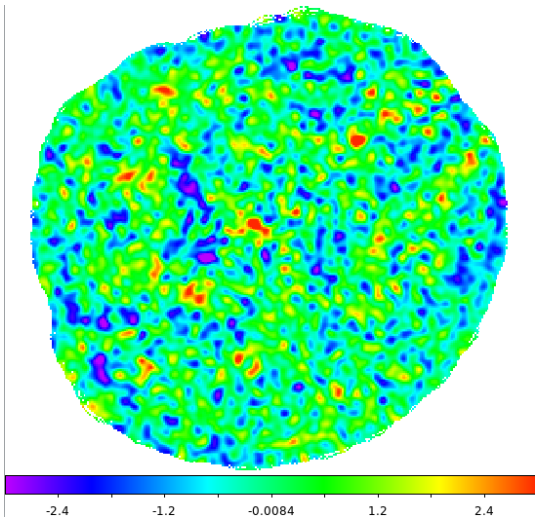

(a) Signal to Noise

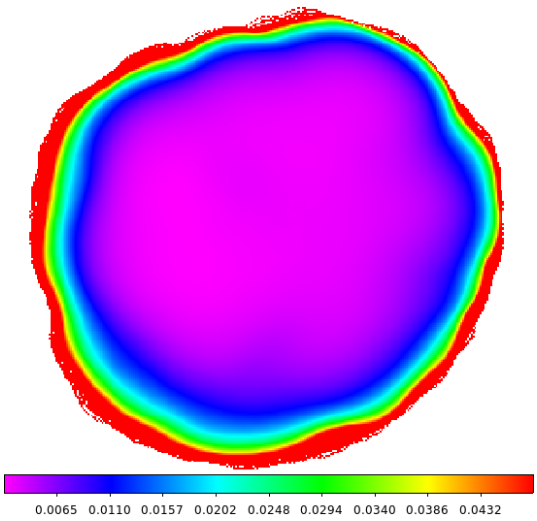

(b) Noise

Figure 4.6: Processing using files that present no anomalies, 'DS9 noise'<0.017, 'Detect noise'<0.07

ber of files (18) used on this process we see way too many peaks, which are very peripheral too. Image noise is pretty higher than the noise in other images too.

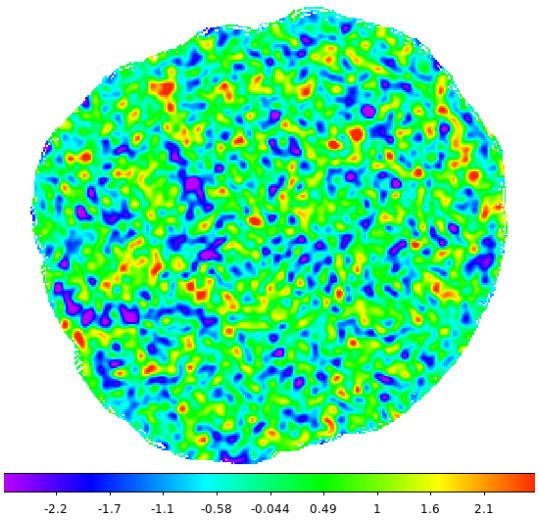

(a) Signal to Noise

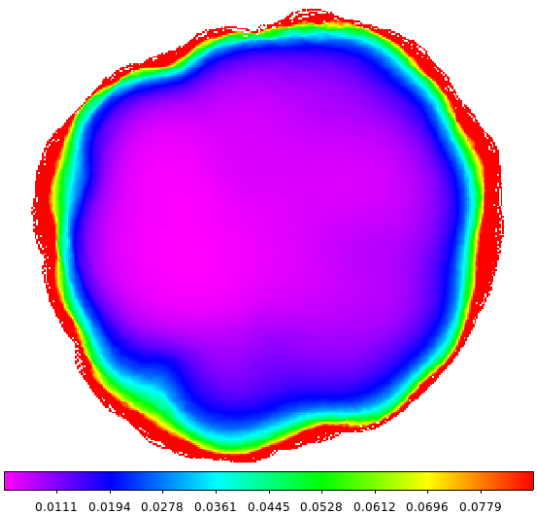

(b) Noise

Figure 4.7: Processing using files that present no anomalies, 'DS9 noise'<0.015, 'Detect Noise'<0.05

Based on this analysis the correct processing appears to be the one corresponding to the fourth result ("no anomalies", "DS9 noise"<0.017, "Detect noise"<0.07) . It is the best result according to noise, both in peaks and in the general image.

4.3.2 Second method

Now, we will process the files based only on 'DS9 noise'. This is the noise in the center of the image, and anomalies and 'detect noise' are data that mainly show us info from the sides of it. As a result of this, we will get images with higher noise on the sides, and these noisy sides will be larger. Though, we will have better results on the center of the image.

First, we can see Fig 4.8, obtained from using only files (93) that have a maximum noise in the center of the image of 0.015 Jy/beam.

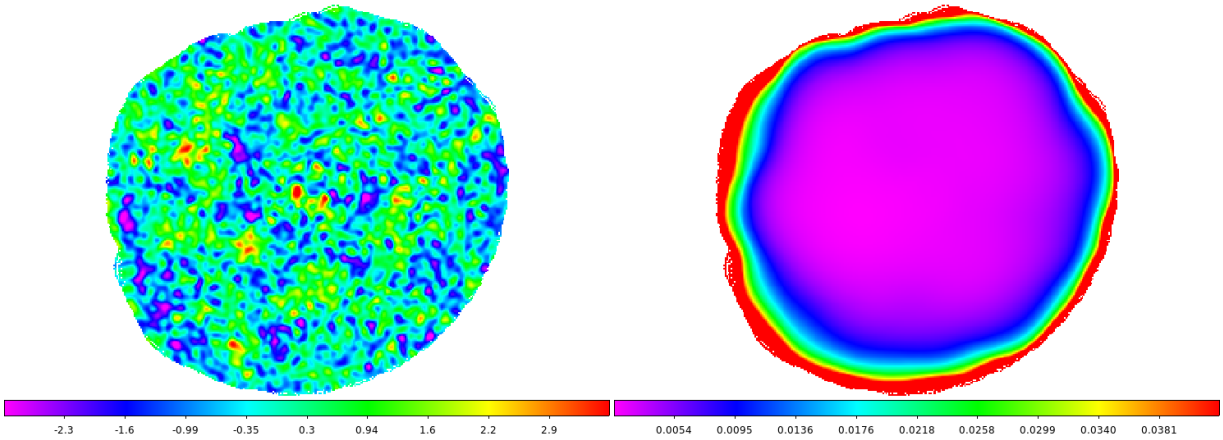

(a) Signal to Noise (b) Noise

Figure 4.8: Processing using files with 'DS9 noise'<0.015

Now, we have Fig 4.9 obtained from the 72 files that have 'DS9 noise'<0.014 Jy/beam.

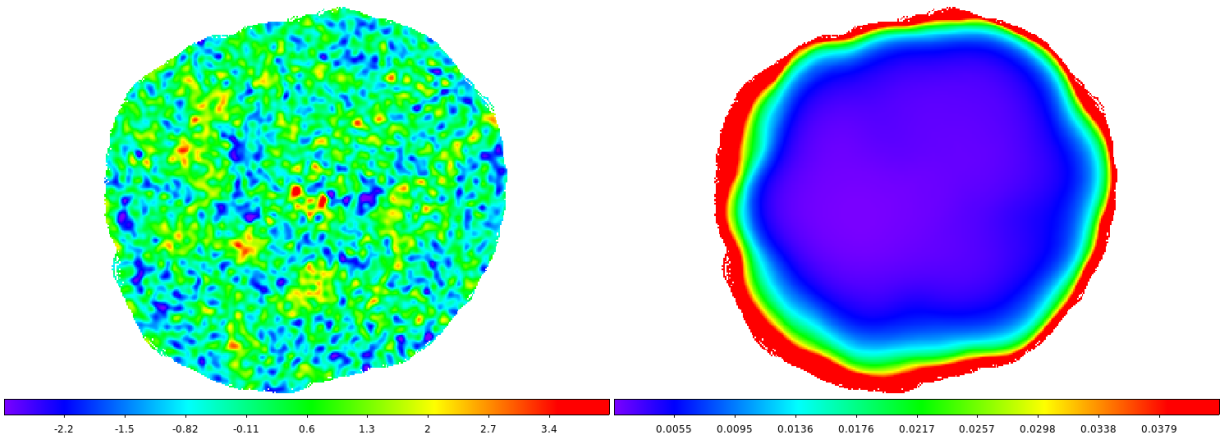

(a) Signal to Noise (b) Noise

Figure 4.9: Processing using files with 'DS9 noise'<0.015

Finally, we have Fig 4.10, an image obtained from the 53 files that present 'DS9 noise' of less than 0.013 Jy/beam.

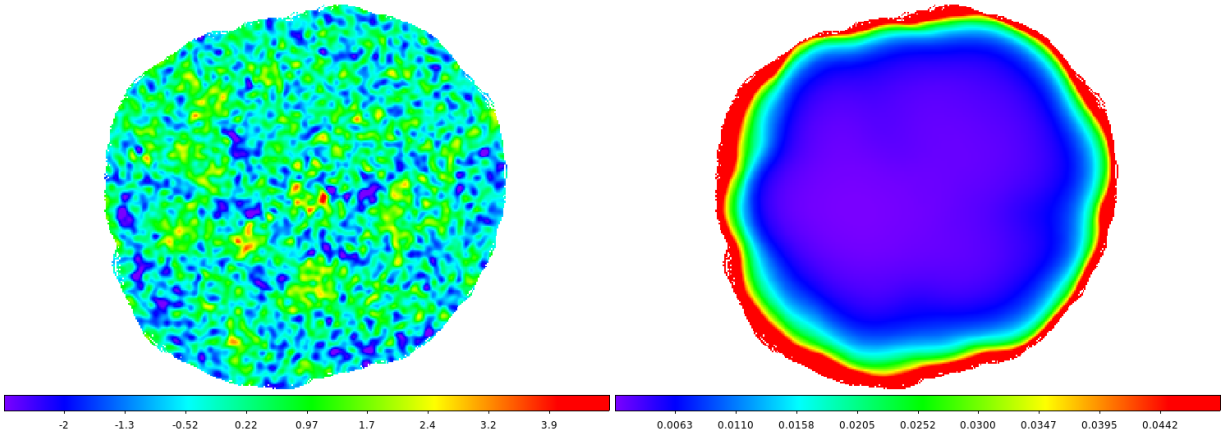

(a) Signal to Noise (b) Noise

Figure 4.10: Processing using files with 'DS9 noise'<0.013

Checking the noise on these pictures we see that the best option from this method is the processing based on 'DS9 Noise'<0.015, showed on Fig 4.8.

Chapter 5

Results

5.1 Resumen

Antes de crear el catálogo realizamos otro nuevo procesado sabiendo ya que archivos tenemos que utilizar para la imagen final. El procesamiento mediante 'deep' es bastante más rápido que si usáramos opciones adicionales como 'faint' o '-final:smooth=halfbeam'. Debido a ello el procesamiento inicial se ha realizado usando solo 'deep'. Una vez explicado esto y conociendo los archivos ideales para realizar la imagen final, usamos las opciones 'deep', 'faint' y 'smooth' de forma combinada.

A pesar de que éste es el método adecuado en principio, finalmente deberemos usar únicamente la opción 'deep' usada anteriormente debido a la falta de resolución de las imágenes proveídas.

Una vez tenemos estas dos imágenes finales correspondientes a ambos métodos ya solo tenemos que crear los archivo .reg en DS9 y señalar las fuentes en la imagen. Para ello utilizamos 'detect' de nuevo, que analizará las imágenes y señalará la ubicación exacta de cada uno de las fuentes.

De estos picos observados tanto en 'DS9' como en 'detect' solo catalogaremos como fuentes los cuáles tengan unos valores de ruido y S/N adecuados (S/N > 3 σ, Noise < 3 mJy) . Además, estas fuentes serán clasificadas como tentativas o robustas en función de su ruido, S/N y su presencia en ambas imágenes.

5.2 Image smoothing

Before buiding the catalog we might do some work to enhance the final image we will work on.

It may be improved using other 'crush' options. We combine the options 'deep' and 'faint' for a result with a higher resolution. Then we may aswell use the option 'smooth' to improve it again.

We firstly use only the option 'deep' because the processing is faster that way than using the complete options. Smoothing options provide more defined images, so the images will be more heavy and complex, which translates into slower processing. Also, when we use 'deep' it might process as one big source what actually are three or four smaller sources, that we will see once we use the combined options.

We may see the improvement on Fig 5.1., Fig 5.2 and Fig 5.3. To highlight these peaks the axis are also modified.

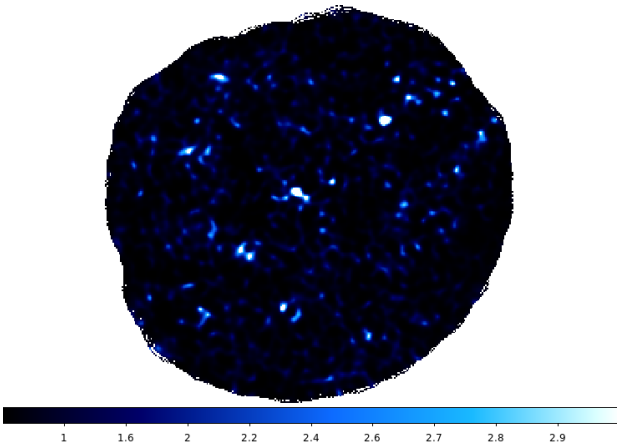

Figure 5.1: Final image using the option 'Deep'

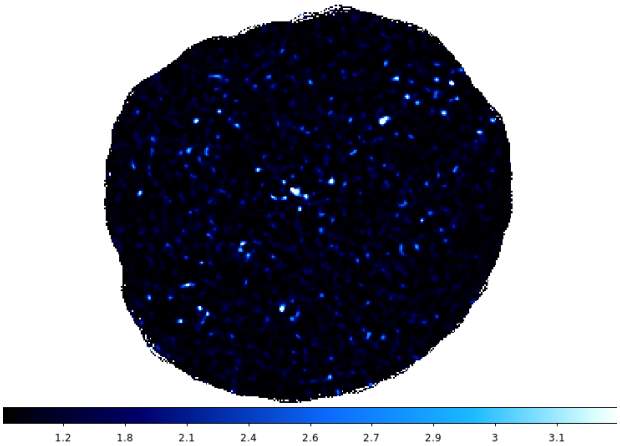

Figure 5.2: Final image using the options 'Deep' and 'Faint'

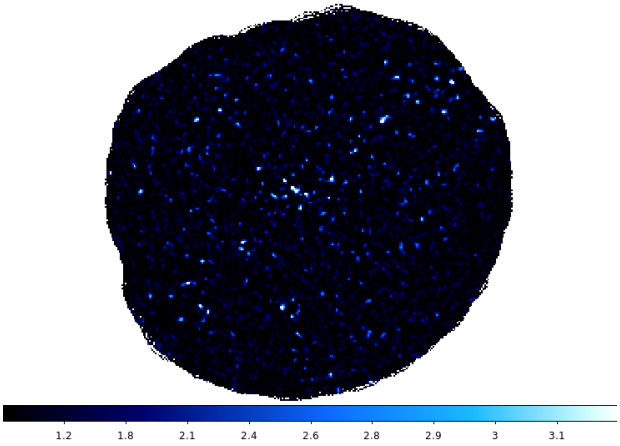

Figure 5.3: Final image using the options 'Deep', 'Faint' and 'Smooth'

5.3 Source extraction

The catalog is presented through a .reg file produced in 'DS9'. We use the data obtained on 'detect' and write it down on the .reg file. For that instance, we classify as sources every peak on the image that surpasses 3 σ. We should not classify the peaks on the borders of the image as sources due to the higher noise present there that might lead to errors. Final result is showed in Fig 5.4.

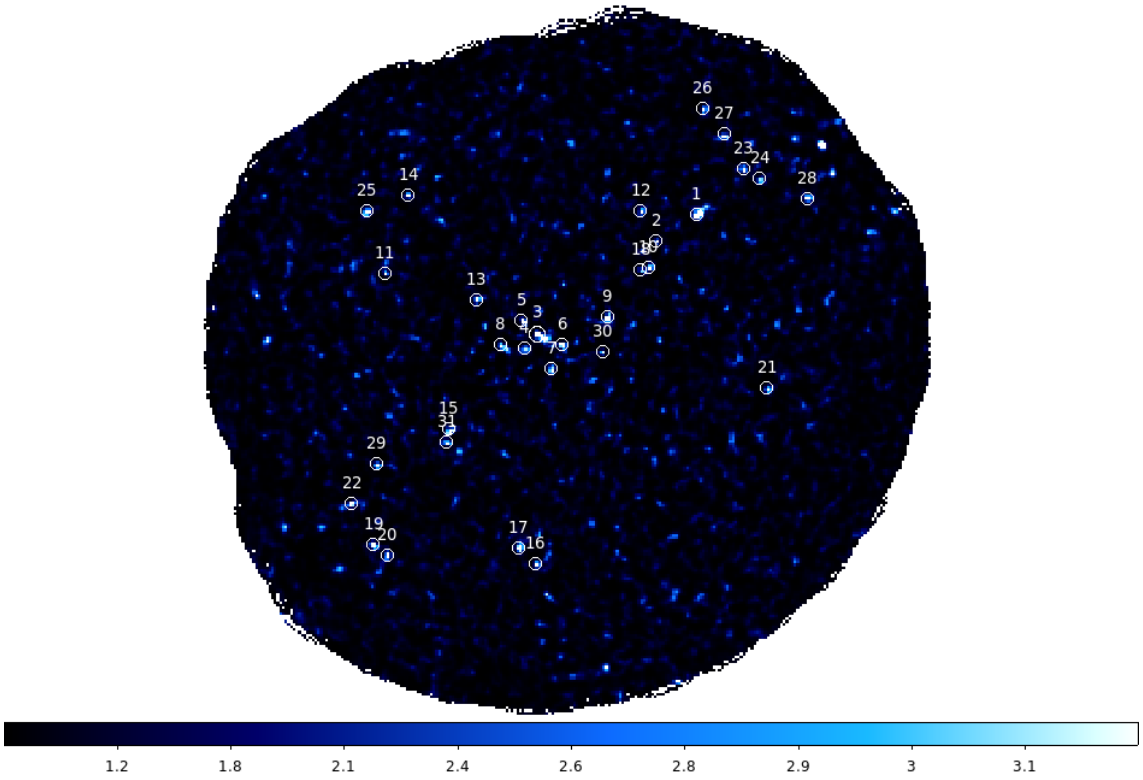

Figure 5.4: Sources found on 'Deep smoothed' process

There is an unexpected overdensity of sources (31). This is due to the process used to get this final result. This process using smoothing makes high-resolution pictures and tries to get data below the detector's actual precision (Angular resolution of 18.6 $''$).

If we do apply the same rules, classifying as a source every peak that surpass the 3 σ value on the regular deep process image we obtained earlier we obtain Fig 5.5.

To classify the data we follow Dannerbauer's et al., (2014) method, classifying sources over 4 σ as robust sources and the ones between 3 and 4 σ as tentative. We will take aswell only the sources with a noise below 3 mJy/beam. We can see the sources found for 'deep' process on the table 5.1.

ID	RA (J2000)	DEC (J2000)	S/N (σ)	Noise (mJy/beam)	Flux (mJy/beam)
FM1	02:24:27.8670	-03:24:02.718	4.587	2.35	10.779
FM2	02:24:12.2009	-03:20:55.906	4.458	2.73	12.17
FM3	02:24:37.7318	-03:26:39.109	3.35	2.09	9.145
FM4	02:24:36.1360	-03:26:54.314	3.21	2.13	6.837
FM5	02:24:30.1882	-03:29:11.160	3.53	4.83	17.045
FM6	02:24:21.4882	-03:23:36.651	3.346	2.47	8.264
FM7	02:24:46.7248	-03:22:16.273	3.277	3.52	11.535
FM8	02:24:41.3569	-03:18:58.614	3.383	9.16	30.988
FM9	02:24:26.1262	-03:24:17.923	3.241	2.39	7.746

Table 5.1: Sources found on 'deep' process using the files obtained from the first method of selection. ID refers to the method used (First Method) and the number of the source showed on the .reg file

The only sources that match our expectations for robust sources are 1 and 2. Also, the sources that we may call tentatives are 3, 4, 6 and 9, for a total of 6 possible sources.

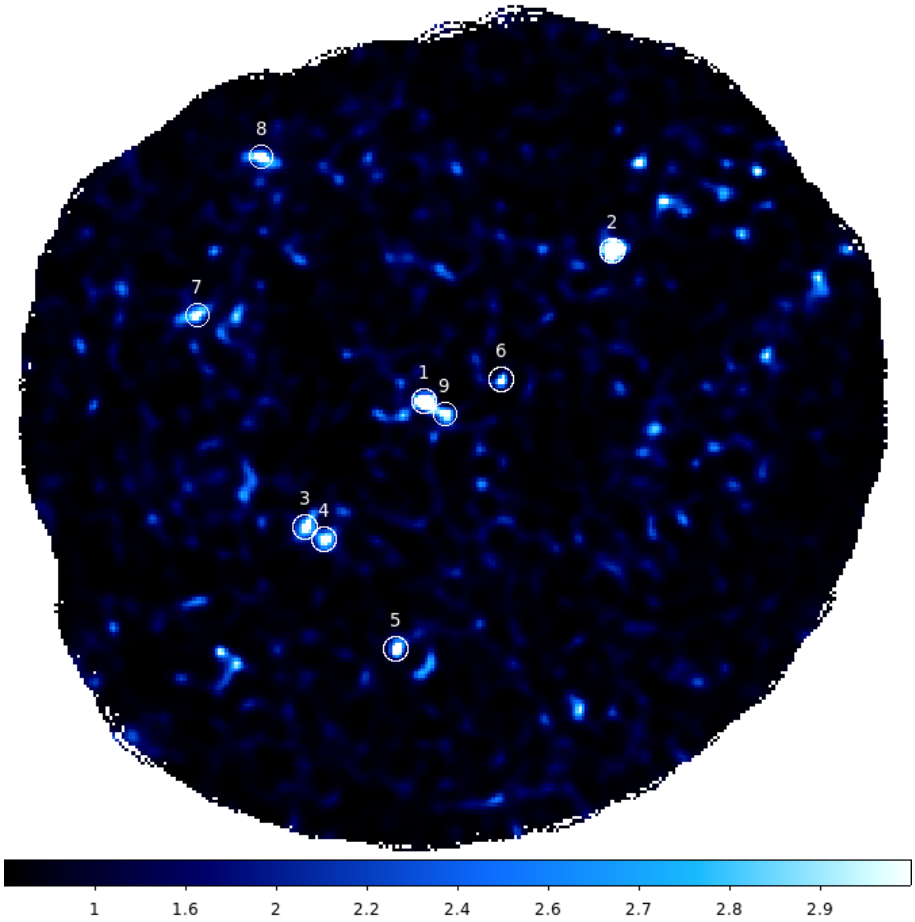

Figure 5.5: Sources found on 'deep' process using the files obtained from the first method of selection

Now, we use as well the file obtained from the second method of data reduction. We can see it on Fig 5.6. This file has 10 sources that peak over 3σ, from which 2 are robust (1 and 2) and other 2 of them are disposable (3 and 7) for having its noise over 3 mJy/beam. We can see the full list on Table 5.2. Therefore, we have 2 robust sources and 6 tentatives.

ID	RA (J2000)	DEC (J2000)	S/N (σ)	Noise (mJy/beam)	Flux (mJy/beam)
SM1	02:24:27.1908	-03:24:16.507	4.613	1.57	7.2424
SM2	02:24:22.1705	-03:24:31.123	4.025	1.7	6.843
SM3	02:24:46.9924	-03:22:15.386	3.569	2.93	10.457
SM4	02:24:43.6457	-03:22:19.566	3.161	1.98	6.259
SM5	02:24:46.9926	-03:22:50.884	3.179	2.84	9.028
SM6	02:24:35.6977	-03:26:46.849	3.255	1.57	5.110
SM7	02:24:38.7666	-03:31:03.683	3.578	11.02	39.429
SM8	02:24:12.4097	-03:20:56.041	3.060	2.17	6.640
SM9	02:24:09.4802	-03:24:37.377	3.0164	2.51	7.571
SM10	02:24:09.9003	-03:19:07.457	3.0164	3.13	9.441

Table 5.2: Sources found on 'deep' process using the files obtained from the second method of selection. ID referes to the method used (Second Method) and the number of the source showed on the .reg file

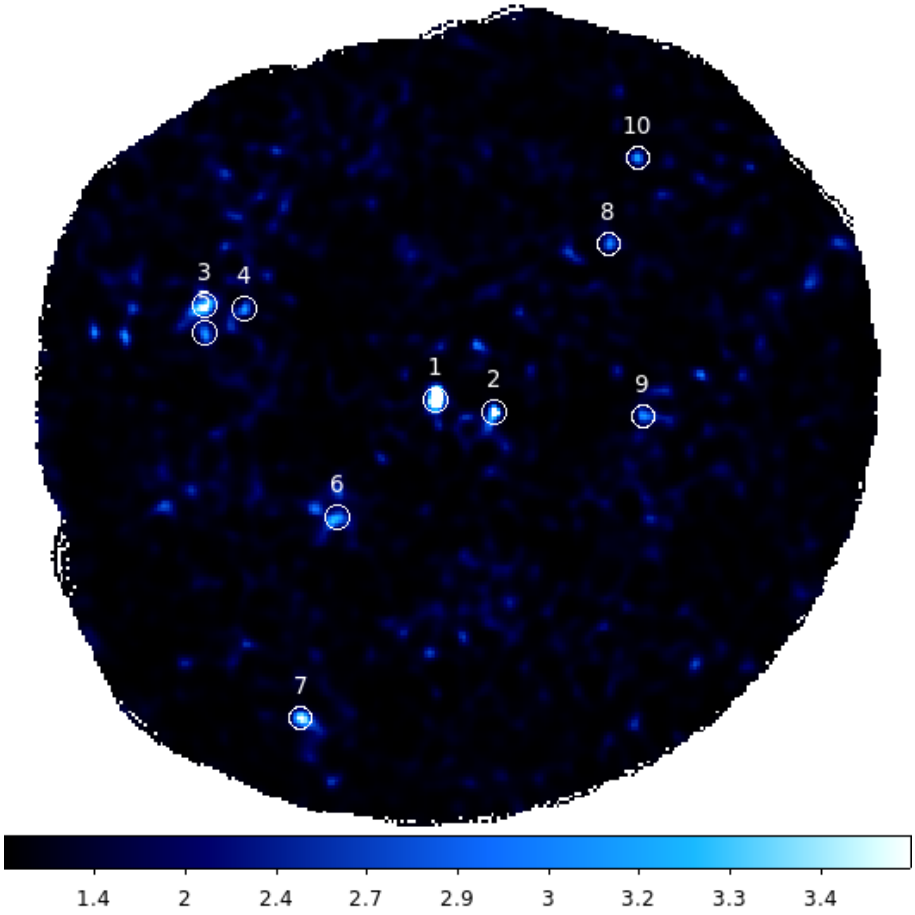

Figure 5.6: Sources found on 'deep' process using the files obtained from the second method of selection

On Fig 5.7 we can see a comparative between these 2 results. We can see how FM1 and SM1 match, which, in addition to it large S/N and it low noise make it a reliable result. Other matched sources are FM6/SM2, FM7/SM3, FM4/SM6 FM2/SM8, that, seeing their good values of noise and S/N, add trust to these results. The location of some of these sources are slightly different but we can still understand them as the same source.

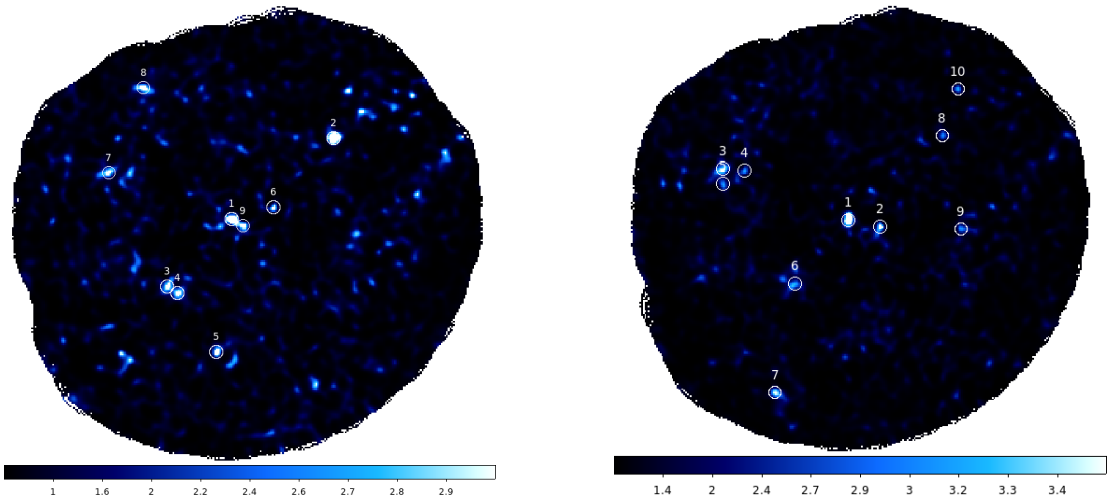

(a) First result

(b) Second result

Figure 5.7: Comparative between both results

Chapter 6

Conclusions

6.1 Resumen

Empezamos este proyecto con el objetivo de buscar "fuentes" en el cluster SpARCSJ022427. Inicialmente se pensaba usar técnicas de "smoothing", ya que los datos pedidos tenían una precisión dada que deberían haber hecho útil este tratamiento. Usando esta técnica obtuvimos 31 fuentes, muchas más de las esperadas, incluso considerando que el procesamiento con smoothing por su extrema finura podía leer como distintas fuentes algunas que en realidad serían una sola. Ante los resultados negativos obtenidos con este método nos vimos obligados a utilizar únicamente el procesamiento 'deep', el cuál ofrece imágenes con menor resolución. El procesamiento deep+faint tenía el mismo problema que el 'deep smoothed'. Inicialmente se esperaba encontrar alrededor 5 fuentes, con este procesamiento y usando ambos métodos de filtrado de archivos hemos obtenido una fuente prácticamente segura (FM1/SM1, superior a 4 σ en ambos resultados con un ruido muy bajo) y otras 4 fuentes que superan 3 σ que coinciden en ambas imágenes con un ruido aceptable (FM6/SM2, FM7/SM3, FM4/SM6 FM2/SM8). Además, existen otras fuentes tentativas que aparecen por separado en los resultados (FM3, FM9, SM4, SM5, SM9) que necesitarían otros estudios para verificar su existencia o no. Por último, pudimos automatizar gran parte del proceso.

6.2 Conclusions

We started this project with the aim of looking for sources (DSFGs) on the cluster SpARCS J0224727 using the data from the LABOCA telescope. We were supposed to use smoothing techniques, since the images asked for this work were asked for a precision that we would later not find. In that first result using the smoothed file we got 31 sources, way more than the ones we could find, even considering smoothing processing diferentiates sources that might be the same. Since we could not use this method we needed to settle on using 'deep' processing for the results, since using 'deep'+'faint' had the very same problem 'deep'+'faint'+'smooth' had. This processing produces images with less resolution. We expected to find around 5 sources, and using both methods of selection we found 1 robust source (FM1/SM1) with more than 4 σ in boths results and a really low noise (<2.35 mJy). Also we found 4 tentative sources (FM6/SM2, FM7/SM3, FM4/SM6 FM2/SM8) that appear on both results, surpass 3 σ and present a good noise (<3 mJy). Additionally, we found 5 more tentative sources (FM3, FM9, SM4, SM5, SM9) that appear in the different results that need other studies to verify its existence. Finally, we could automatize most of the project.

Appendix A

Data tables

ID	TAU mean	'Detect' noise (Jy/beam)	DS9 noise (Jy/beam)	Comment
SpARCSJ022427.45436	0.156	0.0125	0.0521	Wrong
SpARCSJ022427.45437	0.156	0.0122	0.04237	Wrong
SpARCSJ022427.45438	0.156	0.136	0.04625	Wrong
SpARCSJ022427.45439	0.156	0.0122	0.0343	Good
SpARCSJ022427.45440	0.156	0.013	0.06398	Wrong
SpARCSJ022427.45441	0.156	0.0125	0.03797	Wrong
SpARCSJ022427.45442	0.156	0.010	0.0125	Wrong
SpARCSJ022427.45463	0.139	0.011	0.03341	Good
SpARCSJ022427.45465	0.139	0.0109	0.03829	Good
SpARCSJ022427.45466	0.139	0.01	0.03945	Good
SpARCSJ022427.45467	0.139	0.01	0.03563	Good
SpARCSJ022427.45468	0.139	0.0111	0.03743	Good
SpARCSJ022427.45469	0.139	0.011	0.04943	Good
SpARCSJ022427.45470	0.139	0.011	0.03560	Good
SpARCSJ022427.45471	0.139	0.0107	0.03458	Good
SpARCSJ022427.45472	0.139	0.0117	0.04009	Good
SpARCSJ022427.45473	0.139	0.013	0.04006	Good
SpARCSJ022427.45474	0.139	0.014	0.06989	Good
SpARCSJ022427.45475	0.139	0.011	0.03721	Wrong
SpARCSJ022427.45486	0.145	0.015	0.03612	Wrong
SpARCSJ022427.45487	0.145	0.010	0.04093	Good
SpARCSJ022427.45488	0.145	0.011	0.02753	Good
SpARCSJ022427.45489	0.145	0.010	0.03226	Good
SpARCSJ022427.45490	0.145	0.011	0.0123	Good
SpARCSJ022427.45491	0.145	0.011	0.02489	Good
SpARCSJ022427.45492	0.145	0.011	0.03331	Good
SpARCSJ022427.45493	0.145	0.011	0.03880	Wrong
SpARCSJ022427.45508	0.150	0.014	0.06704	Wrong
SpARCSJ022427.45509	0.150	0.017	0.05545	Wrong

Table A.1: Image data

ID	TAU mean	'Detect' noise (Jy/beam)	DS9 noise (Jy/beam)	Comment
SpARCSJ022427.45510	0.150	0.017	0.06382	Good
SpARCSJ022427.45511	0.150	0.017	0.07356	Good
SpARCSJ022427.45512	0.150	0.015	0.06769	Good
SpARCSJ022427.45513	0.150	0.016	0.06591	Good
SpARCSJ022427.45514	0.150	0.017	0.06106	Good
SpARCSJ022427.45515	0.150	0.017	0.06727	Good
SpARCSJ022427.45516	0.150	0.016	0.06668	Wrong
SpARCSJ022427.45517	0.150	0.017	0.06469	Wrong
SpARCSJ022427.45518	0.150	0.017	0.07147	Wrong
SpARCSJ022427.45519	0.150	0.017	0.06813	Wrong
SpARCSJ022427.45760	0.163	0.014	0.06166	Good
SpARCSJ022427.45761	0.163	0.013	0.10500	Wrong
SpARCSJ022427.45762	0.163	0.012	0.08020	Wrong
SpARCSJ022427.45763	0.163	0.013	0.06314	Wrong
SpARCSJ022427.45764	0.163	0.012	0.05332	Wrong
SpARCSJ022427.45765	0.163	0.012	0.06597	Wrong
SpARCSJ022427.45766	0.163	0.010	0.05570	Wrong
SpARCSJ022427.45767	0.163	0.016	0.09969	Good
SpARCSJ022427.45774	0.163			Error
SpARCSJ022427.45775	0.163			Error
SpARCSJ022427.45776	0.163	0.012	0.05336	Good
SpARCSJ022427.45777	0.163	0.013	0.04945	Good
SpARCSJ022427.45778	0.163	0.012	0.06289	Good
SpARCSJ022427.45779	0.163	0.013	0.05909	Good
SpARCSJ022427.45780	0.163	0.013	0.05648	Good
SpARCSJ022427.45781	0.163	0.011	0.05759	Good
SpARCSJ022427.45789	0.161			Error
SpARCSJ022427.45790	0.161			Error
SpARCSJ022427.45791	0.161	0.013	0.06160	Good
SpARCSJ022427.45792	0.161	0.012	0.1124	Wrong
SpARCSJ022427.45793	0.161	0.011	0.08028	Wrong
SpARCSJ022427.45794	0.161	0.012	0.05388	Wrong
SpARCSJ022427.45795	0.161	0.011	0.04321	Wrong
SpARCSJ022427.45796	0.161	0.01	0.04909	Wrong
SpARCSJ022427.45797	0.161	0.01	0.04909	Wrong
SpARCSJ022427.45798	0.161	0.01	0.05763	Wrong
SpARCSJ022427.45799	0.161	0.01	0.04344	Wrong
SpARCSJ022427.45800	0.161	0.01	0.04711	Wrong
SpARCSJ022427.45801	0.161	0.011	0.05988	Wrong
SpARCSJ022427.45802	0.161	0.01	0.04771	Wrong
SpARCSJ022427.45803	0.161	0.01	0.05918	Wrong
SpARCSJ022427.45804	0.161	0.01	0.05335	Wrong
SpARCSJ022427.45840	0.159	0.012	0.06942	Good
SpARCSJ022427.45841	0.159	0.012	0.05525	Wrong

Table A.2: Image data

ID	TAU mean	'Detect' noise (Jy/beam)	DS9 noise (Jy/beam)	Comment
SpARCSJ022427.45842	0.159	0.011	0.05500	Wrong
SpARCSJ022427.45843	0.159	0.012	0.05792	Wrong
SpARCSJ022427.45844	0.159	0.012	0.05581	Good
SpARCSJ022427.45845	0.159	0.014	0.07292	Good
SpARCSJ022427.45846	0.159	0.013	0.06291	Good
SpARCSJ022427.45847	0.159			Error
SpARCSJ022427.45848	0.159	0.015	0.07244	Good
SpARCSJ022427.45849	0.159	0.014	0.06477	Wrong
SpARCSJ022427.46099	0.240	0.015	0.07273	Good
SpARCSJ022427.46100	0.240	0.014	0.06972	Good
SpARCSJ022427.46101	0.240			Error
SpARCSJ022427.46102	0.240	0.012	0.05876	Good
SpARCSJ022427.46103	0.240			Error
SpARCSJ022427.46104	0.240	0.013	0.06008	Good
SpARCSJ022427.46105	0.240	0.013	0.06197	Good
SpARCSJ022427.46106	0.240	0.012	0.05959	Good
SpARCSJ022427.46108	0.240	0.012	0.06116	Wrong
SpARCSJ022427.46109	0.240	0.013	0.06407	Good
SpARCSJ022427.46110	0.240	0.013	0.06047	Wrong
SpARCSJ022427.46111	0.240	0.013	0.05752	Wrong
SpARCSJ022427.46112	0.240	0.012	0.05044	Wrong
SpARCSJ022427.46113	0.240	0.014	0.05593	Good
SpARCSJ022427.46114	0.240	0.014	0.05965	Good
SpARCSJ022427.46115	0.240	0.014	0.05940	Good
SpARCSJ022427.46116	0.240	0.015	0.13010	Good
SpARCSJ022427.46117	0.240	0.014	0.07788	Good
SpARCSJ022427.46118	0.240	0.014	0.06805	Good
SpARCSJ022427.46119	0.240	0.014	0.06591	Good
SpARCSJ022427.46120	0.240	0.014	0.07105	Good
SpARCSJ022427.46121	0.240	0.014	0.07814	Good
SpARCSJ022427.46122	0.240	0.014	0.05825	Good
SpARCSJ022427.46123	0.240	0.014	0.07210	Good
SpARCSJ022427.46124	0.240	0.014	0.06566	Good
SpARCSJ022427.46125	0.240	0.019	0.19380	Good
SpARCSJ022427.46126	0.240	0.014	0.07508	Good
SpARCSJ022427.46127	0.240	0.014	0.06442	Good
SpARCSJ022427.46128	0.240	0.014	0.06688	Good
SpARCSJ022427.46129	0.240	0.017	0.08844	Good
SpARCSJ022427.46130	0.240	0.014	0.06081	Good
SpARCSJ022427.46131	0.240	0.014	0.06247	Good
SpARCSJ022427.46137	0.240	0.015	0.07518	Good
SpARCSJ022427.46138	0.240	0.014	0.05504	Good

Table A.3: Image data

ID	TAU mean	'Detect' noise (Jy/beam)	DS9 noise (Jy/beam)	Comment
SpARCSJ022427.46139	0.240	0.014	0.06128	Good
SpARCSJ022427.46140	0.240	0.015	0.06542	Good
SpARCSJ022427.46141	0.240	0.016	0.10400	Wrong
SpARCSJ022427.46142	0.240	0.015	0.05779	Wrong
SpARCSJ022427.46143	0.240	0.015	0.08309	Good
SpARCSJ022427.46144	0.240	0.014	0.06737	Wrong
SpARCSJ022427.46145	0.240	0.015	0.07480	Good
SpARCSJ022427.46146	0.240	0.015	0.07995	Wrong
SpARCSJ022427.46147	0.240	0.029	0.14620	Wrong
SpARCSJ022427.46148	0.240	0.015	0.06603	Wrong
SpARCSJ022427.46149	0.240	0.016	0.07887	Good
SpARCSJ022427.46150	0.240	0.017	0.07789	Wrong
SpARCSJ022427.46151	0.240	0.017	0.07790	Good
SpARCSJ022427.46152	0.240	0.018	0.08632	Good

Table A.4: Image data

Appendix B

Scripts

B.1 Crush script

Script that process all images we have on a certain folder with settings to choose

```
##### Applying crush to every individual file

import subprocess
import os

### We need to set ourselves in the directory where we have all our data

os.chdir("/home/armando/Downloads/crush-2.41-3/crush/TFG/rawdata/")

# Also we are going to write the output on an ascii file that we now
# open and later we will open it, python wil read it as a list

file = open('files', 'w')

result = subprocess.run('ls', stdout=file)

file.close()

f = open('files', 'r')

data = f.read()

f.close()

# Now it has served to our purpose we delete it

os.remove('files')
```

```
### We have to change manually the days and the code of the data we have

d1 = data.replace("-2015-07-29-C-095.F-9711A-2015", "")

d2 = d1.replace("-2015-07-28-C-095.F-9711A-2015", "")

d3 = d2.replace("-2015-07-27-C-095.F-9711A-2015", "")

d4 = d3.replace("-2015-08-26-C-095.F-9711A-2015", "")

d5 = d4.replace("APEX-", "")

lista = d5.replace("files", "")

### We now go to where we have installed crush

os.chdir("/home/armando/Downloads/crush-2.41-3/crush/")


### Where the options are -deep, -bright, -faint-, -extended,
### -final:smooth=halfbeam and sourcesize=x and we have the option
### to combine them.

for l in lista:
    subprocess.run(['./crush', 'laboca', '-deep', l], stdout=subprocess.PIPE)
```

B.2 Detect script

With this script we get printed in the terminal the results of the 'detect' feature

```
#######Detect for every file

#First we need to have a python list of every file we are gonna use.

import subprocess
import os

#We need to set ourselves in the directory where we have all our data

os.chdir("/home/armando/Downloads/crush-2.41-3/crush/TFG/rawdata/")
```

```
#Also we are going to write the output on an ascii file that we now open

file = open('files', 'w')

result = subprocess.run('ls', stdout=file)

file.close()

f = open('files', 'r')

data = f.read()

f.close()

os.remove('files')

###We have to change manually the days and the code of the data we have

d1 = data.replace("-2015-07-29-C-095.F-9711A-2015", ".fits")

d2 = d1.replace("-2015-07-28-C-095.F-9711A-2015", ".fits")

d3 = d2.replace("-2015-07-27-C-095.F-9711A-2015", ".fits")

d4 = d3.replace("-2015-08-26-C-095.F-9711A-2015", ".fits")

### Now we write the directory where we have the FITS files.

d5 = d4.replace("APEX-",
"~/Downloads/crush-2.41-3/crush/TFG/newdata/SpARCSJ022427.")

lista = d5.replace("files", "")

#We now go to where we have installed crush

os.chdir("/home/armando/Downloads/crush-2.41-3/crush/")

file_ = open('output', 'w')

#Now we check the data and write it down
for l in lista:
    resultado = subprocess.run(['./detect', 's2n=3', l], stdout=file_)
```

```
    resultado.stdout

file_.close()

#Now we should have the result of every detect saved in a txt file called
#output in the crush folder. Also all the results will be printed in the
#terminal, we shall just copy and paste them.
```

B.3 Selection script

Script that will make the final cut, selecting those files with least noise

```
###Program to select the files that will make the best final image possible
###and process them

#First we import the astropy module and his ascii utility (it is imperative
#to have astropy downloaded).

from astropy.io import ascii

#Now we import the .dat file into python. We must specify the separations
#between columns.

data = ascii.read("listanoise.dat", delimiter="\t")

#Now we filter the data. In this case I've chosen to set the limits on
#0.015 for the noise on the sources, 0.07 for the minimal noise detected
#on DS9 and allowing no strange objects on the images.

filter = data[(data['NOISE']<0.015) & (data['MINNOISE']<0.07) &
(data['COMMENT']=="Correct")]

#Finally we save an ascii file with the files that are suitable to use
#following the previous filter.

ascii.write(filter['ID'], 'VALUES.DAT', overwrite=True)

#Now we import that file again, this time using a simpler method since
#we do not need columns.

f = open('VALUES.DAT', 'r')

data = f.read()
```

```
f.close()

import os

os.remove("VALUES.DAT")

#We have the result as 'data' so we now just replace the "SpARCSJ022427."
#for nothing

data1 = data.replace("SpARCSJ022427.", "")

#Now we eliminate the 'col' line coming from astropy

lista = data1.split()

mitad = int(len(lista)/2)

lista1 = lista[mitad:]

lista2 = ' '.join(lista1)

#Now we write down the command we are using with our crush settings and
#make it an ascii file ready to execute.

#Where the options are -deep -faint -extended -bright -show
#5-sourcesize=x -finalsmooth=halfbeam

exe = "./crush laboca -deep -finalsmooth=halfbeam "  + lista2

files = open('executable.dat', 'w')

files.write(exe)

files.close()


#Now we just have to execute this file (chmod +x executable.dat,
#./executable.dat)
```

List of Figures

2.1 Apex Telescope 8
2.2 LABOCA bolometer array. 9

4.1 APEX-45439 file, processed through different options 14
4.2 Anomaly on APEX-45436 15
4.3 Processing using all files 15
4.4 Processing using all files that present no anomalies 16
4.5 Processing using files that present no anomalies, 'DS9 Noise'<0.018, 'Detect Noise'<0.09 . 16
4.6 Processing using files that present no anomalies, 'DS9 noise'<0.017, 'Detect noise'<0.07 . . 17
4.7 Processing using files that present no anomalies, 'DS9 noise'<0.015, 'Detect Noise'<0.05 . . 17
4.8 Processing using files with 'DS9 noise'<0.015 18
4.9 Processing using files with 'DS9 noise'<0.015 18
4.10 Processing using files with 'DS9 noise'<0.013 19

5.1 Final image using the option 'Deep' 21
5.2 Final image using the options 'Deep' and 'Faint' 21
5.3 Final image using the options 'Deep', 'Faint' and 'Smooth' 21
5.4 Sources found on 'Deep smoothed' process 22
5.5 Sources found on 'deep' process using the files obtained from the first method of selection . 23
5.6 Sources found on 'deep' process using the files obtained from the second method of selection 24
5.7 Comparative between both results 24

Bibliography

Blain et al., 2002. *"SUBMILLIMITER GALAXIES"*. Physics Report. 369 (2002) 111-176

Casey et al., 2014. *"DUSTY STAR-FORMING GALAXIES AT HIGH REDSHIFT"*. Physics Reports 541 (2014) 45–161

Chapman et al., 2001. *"SUBMILLIMITER IMAGING OF A PROTOCLUSTER REGION AT Z = 3.09"*. The Astrophysical Journal, 548:L147-L151, 2001

Dannerbauer et al., 2014. *"AN EXCESS OF DUSTY STARBURSTS RELATED TO THE SPIDERWEB GALAXY"*. Astronomy Astrophysics, Volume 570, A55 (2014)

Kovács et al., 2006 *"SHARC-2 350μ m OBSERVATIONS OF DISTANT SUBMILLIMITER-SELECTED GALAXIES AND TECHNIQUES FOR THE OPTIMAL ANALYSIS AND OBSERVING OF WEAK SIGNALS"* Caltech PhD thesis

Kovács et al., 2008. *"CRUSH: FAST AND SCALABLE DATA REDUCTION FOR IMAGING ARRAYS"*. Proc. SPIE, 7020, 45.

Kratsov et al., 2012. *"FORMATION OF GALAXY CLUSTERS"*. arXiv:1205.5556v1

Lineweaver et al., 2003 *"INFLATION AND THE COSMIC MICROWAVE BACKGROUND"*. The New Cosmology, pp. 31-65 (2005)

Siringo et al., 2009. *"THE LARGE APEX BOLOMETER CAMERA LABOCA"*. Astronomy and Astrophysics, Volume 497, Issue 3, 2009, pp.945-962